UNIVERSITÉ PARIS 13

ÉCOLE NORMALE SUPÉRIEURE

MASTER INTERNSHIP REPORT

Set-up of a new laser system for a quantum magnetism experiment

Author:
Youssef AZIZ ALAOUI

Supervisor:
Dr. Laurent VERNAC

June 20, 2019

Acknowledgements

I would like to express my heartfelt gratitude to Laurent with whom I spent most of my time these past few months.
My sincere thanks go to Bruno who welcomed me in this great group.
I am thankful to all other members of the team with whom I had great interactions all throughout my internship.
Not to be forgotten, Fabrice of the electronic workshop who demonstrated stupendous reactivity and provided us with a most precious help.
I am also grateful towards Sylvie Spielmann of the administrative team, and of course towards Mr. David Papoular (DJ) who advised me to visit the *Laboratoire de Physique des Lasers* in the first place.

...

Contents

List of Abbreviations

MO	**M**aster **O**scillator
MD	**M**aster **D**iode
TA	**T**apered **A**mplifier
SMOF	**S**ingle **M**ode **O**ptical **F**iber
PDH	**P**ound **D**rever **H**all
FP	**F**abry **P**érot
FP	**F**abry **P**érot **C**avity
ULE	**U**ltra **L**ow **E**xpansion
EOM	**E**lectro **O**ptical **M**odulator
FSR	**F**ree **S**pectral **R**ange
PID	**P**roportional **I**ntegrator **D**erivator
OBE	**O**ptical **B**loch **E**quations
PBS	**P**olarizing **B**eam **S**plitter
IR	**I**nfra **R**ed

Introduction

As part of the ICPF master's degree curriculum, I was welcomed within the *Laboratoire de Physique des Lasers* of *Université de Villetaneuse*, in the *Gaz Quantiques Magnétiques* team. Under the supervision of Dr. Vernac Laurent, I worked on the installation of a new laser system for the Chromium experiment.
The current purpose of the experiment is to investigate the dynamics of entanglement growth between Chromium atoms trapped in optical lattices. The trapping process involves several atomic transitions, all of which are summarized in the following picture.

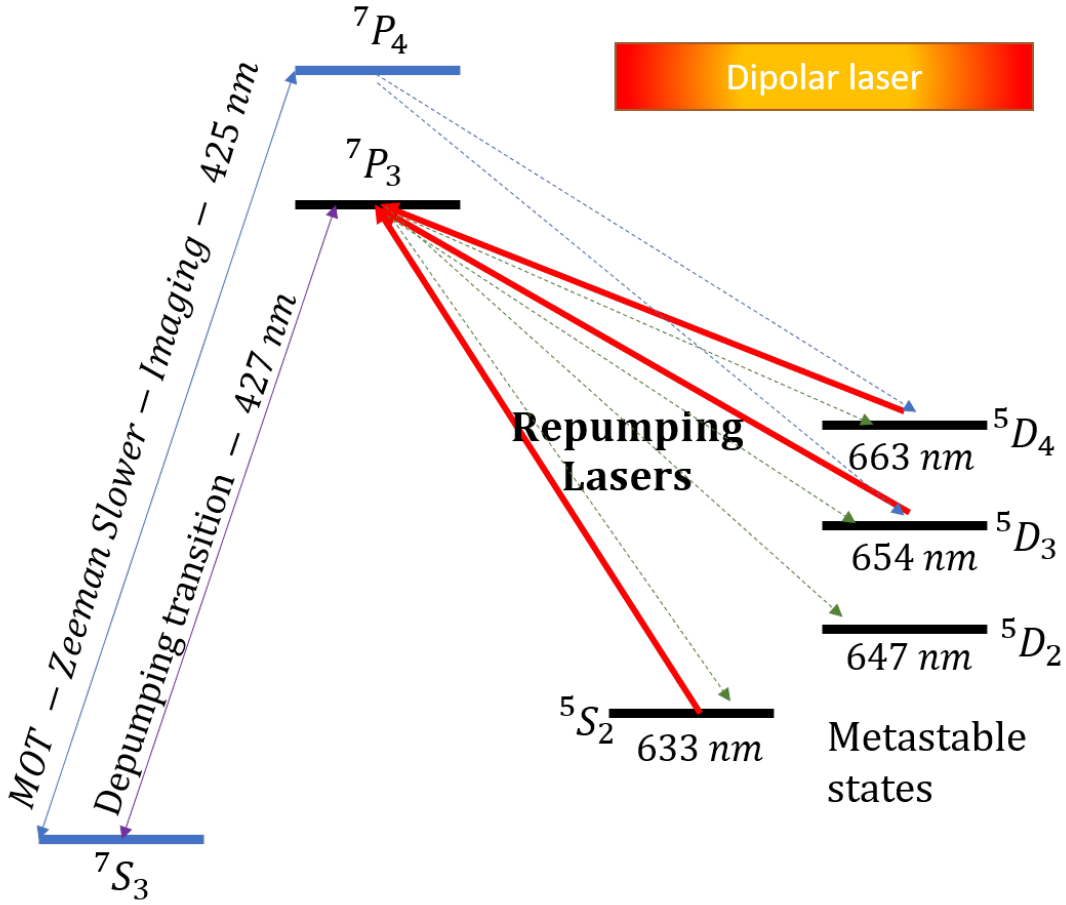

FIGURE 1: Relevant transitions of the bosonic isotope of Chromium. The nuclear Spin is zero, therefore it shows no hyperfine structure.

The condensation scheme follows as such: First, the MOT, Zeeman slower, *depumper* and the dipolar laser are activated. *Repumpers* are then switched on to accumulate atoms in the $^7S_3$ ground state while the MOT, the Zeeman slower and the *depumper* are switched off, then all atoms are optically pumped into the $M_s = -3$ state. Upon which the evaporative cooling starts while the dipolar laser which now forms a cross pattern allows for the condensation in the center of the cloud.

In the scheme above the 425.5 nm laser used both for cooling the Chromium atoms and imaging them was initially produced through frequency doubling of a (851.1 nm/1.5 Watt) Sa: Ti laser. This laser is intrinsically stable and powerful enough, however, it came with prohibitive maintenance costs, moreover its frequency displayed small fluctuations during the imaging process because of closing mechanical shutters placed on the same optical bench.
As one would guess, frequency stability is of the utmost importance for the accuracy of the imaging process (chap. 2), and therefore the monitoring of quantum entanglement dynamics.
For both these reasons, it was decided to set up a new laser system composed of a Master Diode (MD) producing a 30 mW laser beam at 851.1 nm and a Tapered Amplifier (TA) used to reach power levels comparable to those of the Sa: Ti laser. This new system is easier to maintain and insensitive to the closing of the shutters (Chap.1 and fig.1.2).

During this internship, we indeed succeeded in replacing the initial setup by a fully operational MD/TA system. In particular my work consisted in the :

- Frequency stabilization of the new laser through the Pound Drever Hall (PDH) method using a Fabry Perot Cavity as a stable reference
- Optimization of the power amplification process
- Optimization of the frequency doubling process

As it turns out, because of the replacement of the Sa: Ti laser, we also had to find new means of locking the 663 nm repumper diode (fig.1), this we did injecting it in the same cavity as the new 851 nm diode.

In parallel to these experimental adventures, I characterized, through numerical simulations, the impact of laser frequency fluctuations on the accuracy of the absorption imaging system used in the Chromium experiment (chap.2).

Chapter 1

Experimental Achievements

1.1 Master oscillator characterization

The Master Diode is the first building block of the new laser system we installed. This particular MD is a frequency stabilized laser diode, it is stabilized using a Littrow type external cavity, its theoretical linewidth is evaluated to 50 kHz.
For intensity and frequency stability, it is important to minimize the lasing threshold of the diode: adjusting the tilt and angle of the diffracton grating, we reached a working threshold of 54 mA. Currently the diode is working at 130 mA input current.
Following the minimization of the intensity threshold, we characterized the MD laser mode.

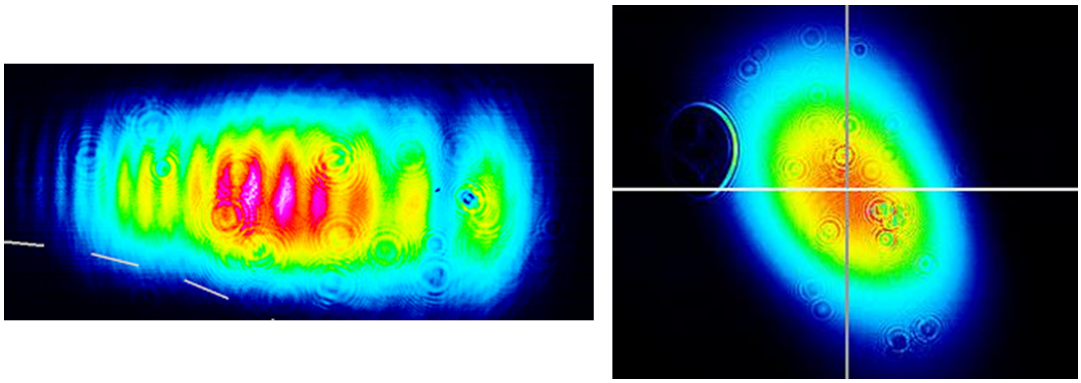

FIGURE 1.1: Left: The MD initial output mode. Right: the final output mode after setting up the adequate cylindrical telescope fig. 1.2. The telescope's lenses were chosen to produce as circular a mode as possible i.e. the best suited to the fiber leading to the tapered amplifier. The distance between the telescope's lenses was chosen to best collimate the laser beam. At 150 cm from the telescope the $\frac{1}{e^2}$ radii are 1014 and 1115 μm.

This data was of importance in that it helped adequately injecting the laser in the single mode fiber leading to the tapered amplifier (fig. 1.2).

1.2 Construction of the optical setup

Atomic cooling and imaging require powerful laser sources, likewise the same laser sources should display a good frequency stability.
By itself, the Master Oscillator does not fulfill any of the conditions needed for proper cooling or imaging of the Chromium atoms, in particular we need at least 300 mW of blue light at 425.5 nm (**frequency accuracy and stability requirements**).

For this we need an infrared power of approximately 1.5 W (at 851 nm) **(power requirement**). Fulfillment of these three experimental requirements led us to the construction of three optical *"paths"* :

- The amplification and frequency doubling path
- The frequency locking path
- The wavelength measurement path

All of these paths are represented in the schematics next page 1.2.

1.3 Master Oscillator frequency locking

All lasers demonstrate frequency wander at some level, it is primarily due to temperature variations, and laser gain dynamics. The Pound-Drever-Hall (PDH) technique allows for the stabilization of laser light frequency using a stable cavity as a reference.
In this internship, we used an ultra low expansion (ULE) cavity as a reference. It uses a material which expansion coefficient changes sign at a given temperature (around 20 °C in theory), the cavity is subjected to a servo loop locking it to this critical temperature (10 mK precision). This ensures a *constant* cavity length, and all in all, a stable laser frequency.

More specifically, one takes advantage of the fact that the reflection function of a Fabry Pérot cavity depends evenly on frequency. This means that the derivative of the reflection function is an odd function of frequency across the resonance. Therefore a measurement of this derivative can be fed back to the laser to hold it on resonance.
In order to implement the PDH method, one can use an electro optic modulator. An EOM is basically a crystal whose refractive index can rapidly change in response to an electrical stimuli. This index variation will imprint a phase modulation on any light wave travelling the crystal medium. In this way, the laser we use can be phase modulated, in particular a sinusoidal phase modulation will add mainly two sidebands (an infinity in fact with decreasing amplitudes) to the spectral decomposition of the laser light.
Imagine then a laser modulated so that the light now carries three frequencies : the carrier at $4.42910^{15} Hz$, and two other frequencies (at $\pm 25 MHz$ from the main one in our case) which constitute so-called side-bands.
These sidebands do not have the same frequency as the incident beam, but do have a definite phase relation with it. If we interfere the sidebands with the fundamental component of the reflected beam for example, the sum displays a beat pattern at the modulation frequency which can be collected and analyzed using a phase shifter, a mixer and a low pass filter. The phase of the beat pattern gives the phase of the reflected beam, thus informing us on the position of the laser frequency with respect to the cavity resonance.[1]

Practically: the implementation of the PDH method required a preliminary adjustment of the MD's wavelength, the merit criteria for the wavelength adjustment is the monomodal nature of the light and the mode stability of the diode around the target wavelength (851.10(5/6) nm): in the ideal case mode jumps must not occur in a 10 pm range around the central wavelength, which can be achieved tuning the

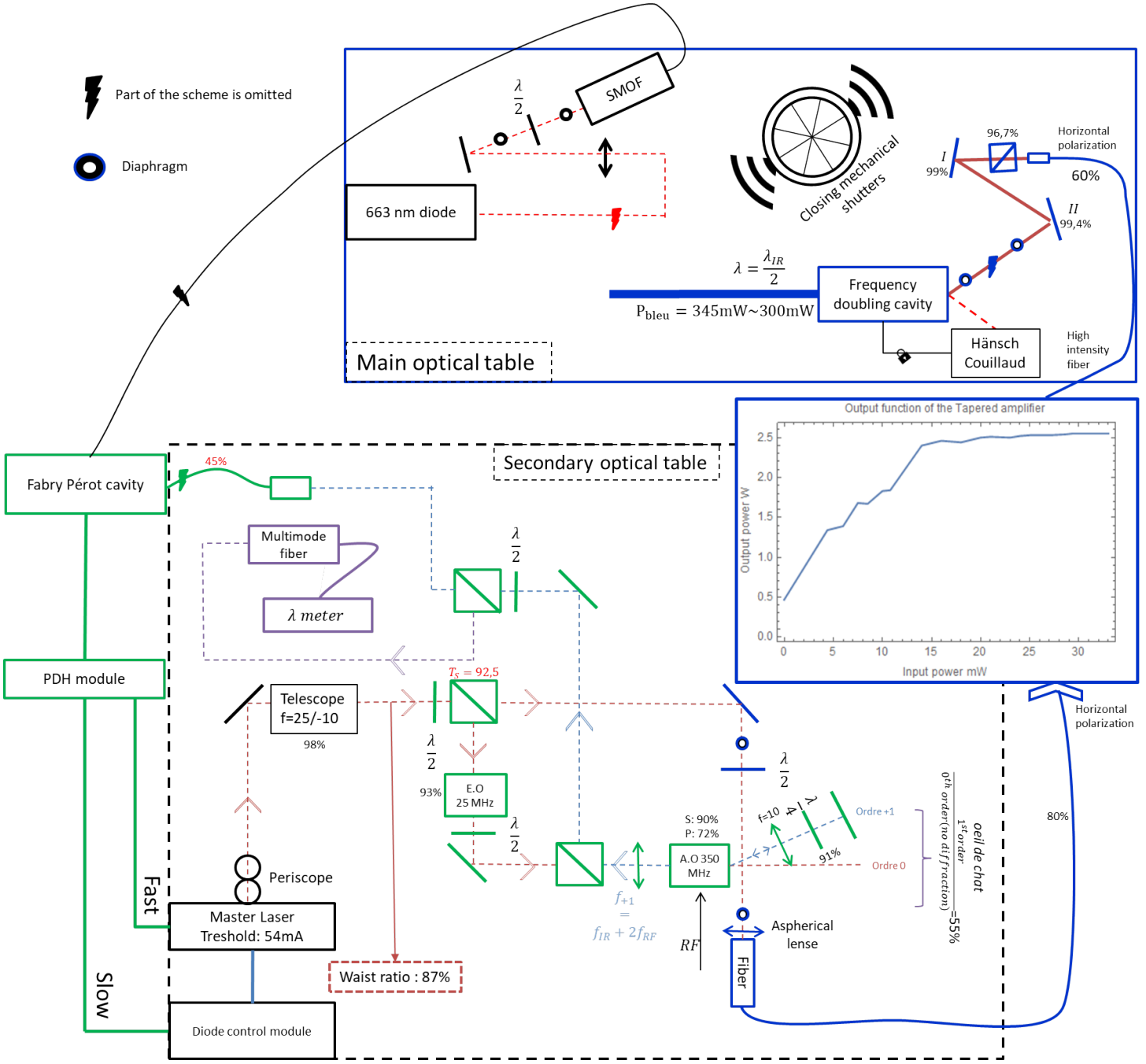

FIGURE 1.2: The optical setup built during the internship. The *"starting point"* (the MD) bottom left corner of the schematics. The 851.1nm laser produced by the MD is mode adapted using a telescope. The laser is then split into two parts of unequal power. The first part (few mW) follows the locking path in green (EO+AOM) and is further split into two parts one of which goes to the wavemeter (purple) and gives us the value of the laser's wavelength (to picometric precision), the other goes to the FPC and serves the actual locking purpose (sec.1.3). The most powerful part of the laser (25-30 mW) follows the amplifying and frequency doubling path in blue.

diode cavity temperature (and thus its length), the injected current (into the diode) and the angle of the diffraction grating.
The MD laser is then directed towards the ULE cavity.
The signal reflected off the cavity and onto the photo-diode (cf. fig. 1.2) is transmitted to the PDH module, a component which allows us to create, shape and refine the error signal by tuning three parameters (CH0: The amplitude of the demodulation signal sent to the multiplier / CH1: The amplitude of the modulation sent to the EO and also the relative phase between both). In particular, we took care of centering the PDH error signal and symmetrizing it. It is this error signal which serves the actual locking purpose. Once the signal shape was satisfying, we checked the actual locking.
Ideally locked signals should feature a constant amplitude, in our first locking trial however, remnant oscillations were still observed, an issue we fixed by lowering the gain of the integrator module of the PID controller and changing the capacity of the relevant capacitors. We checked through Fourier transform the absence of remnant oscillations in the locked signal.

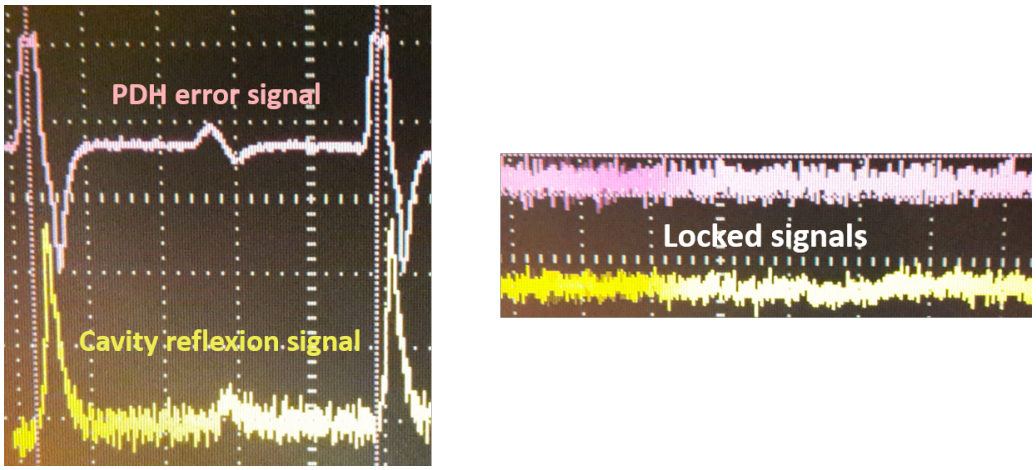

FIGURE 1.3: Left: The PDH error signal and cavity reflection peaks of the 851.1 nm laser for slow modulation. Right: The residual frequency fluctuations are evaluated to less than ($\simeq$) 0.4 MHz.

1.4 Tapered Amplifier output power optimization

Having locked the master diode frequency through the PDH method, we took care of the power requirement explicited in 1.2. This we did by injecting the output laser into a polarization maintaining, single mode optical fiber (SMOF) leading to a tapered amplifier (Toptica Boosta PRO). The main goal of this amplifier was to increase the power of the MD output to figures comparable with those of the Sa: Ti we aimed to replace.
As far as the injection into the SMOF is concerned, thanks to a sound choice of the injection lens and through a delicate adjustment of the lens to fiber distance we reached an 80% output efficacy, an excellent ratio.
We then used a specifically designed *fiber input port*, to link the fiber to the tapered amplifier. The TA beam goes through a double stage optical isolator (Transmittance=85%) and is then connected to a high power tolerant fiber, fine tuning all available degrees of freedom, we reached a final output efficiency of 60% for this

one fiber. The TA not producing a Gaussian mode, this coupling is quite good.
The typical output power of the system is 1.5 W, which is equal to that of the Sa: Ti laser at maximum efficiency, moreover this system displays an output power plateau for input powers higher than 15 mW (fig. 1.2), which is a great stability feature.
The tapered amplifier was then fitted within **the main optical bench** . The fluctuations of the TA laser's frequency are only linked to the inner workings of the **master diode**, which sits still **in the secondary bench**. It is therefore unperturbed by the mechanical shutters of the main optical table (fig. 1.2).
Besides frequency fluctuations, though the setup showed great power stability, some power fluctuations were still to be observed (2% in relative terms) despite the use of a polarizing beam splitter (PBS) and should be solved through proper polarization maintaining, i.e. by better aligning the light polarization with one of the neutral axes of the fiber with a zero order $\lambda/2$ waveplate.

1.5 The frequency doubling process.

The power issue having been taken care of, we focused on the frequency doubling process necessary for a good interaction between the light and the atoms.
The frequency doubling occurs in an external four-mirror ring commercial cavity (model FD–SF–07), produced by Tekhnoscan. The second harmonic is generated in a 15-mm-long lithium triborate (LBO) crystal.
The efficiency of the doubling mechanism depends on the quality of the laser injection into the cavity. Since the Sa: Ti laser was already injected into said cavity, we started by aligning the new TA beam with it and checked the correspondence between the two modes.
Due to the careful choice of the collimating lens of the TA output fiber, the two modes showed good correspondence, in fact the DM/TA system produces a laser of lower ellipticity, these features allowed us to correctly inject the TA output into the doubling cavity.

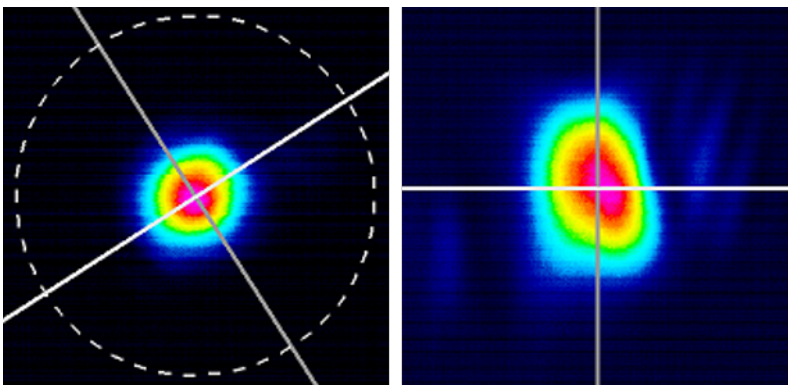

FIGURE 1.4: Comparison of both laser modes. Left : MD/TA laser beam. Right : the Sa: Ti mode. For practical reasons both modes have not been characterized at the exact same position in the *optical path*, however at 54 cm from the output fiber the two waists of the TA laser are respectively 500 and 530 μm, while those of the Sa: Ti are measured to 405 and 580 μm at 60 cm (pictures are not on the same scale). These distances correspond to the rough position of the injection lens.

We then proceeded to the optimization of the doubling process. This optimization followed a two stage adjustment: First, the usual beam-work : aligning the TA laser with the Sa: Ti beam ensured a *good* cavity injection, and a finer adjustment of the mirrors I and II (1.2) orientation allowed for the centering of the beam and the elimination of odd modes components (odd relative to the projection of the laser mode on those of the cavity).
The second stage consisted in a more precise mode adaptation through the fine tuning of the collimation lens distance from the fiber's output face. The typical blue light power is 330 mW.

We should report here that the cavity length is itself subjected to a servo-loop based on the Hänsch Couillaud method. The Hänsch Couillaud method is a polarization sensitive locking technique. Here it allows us to control the doubling cavity length through a piezoelectric component so that the IR laser stays resonant, this guarantees that slow and small amplitude drifts of the IR laser do not affect the production of the 425.5 nm light too greatly.
An interesting observation was that of the extreme dependency of the Hänsch Couillaud error signal on the polarization of the infrared laser at 851.105 nm, in particular its offset varied periodically as the polarization did too, this problem we solved by using a cleanup PBS after the output of the high power tolerant fiber.

Though we succeeded in doubling the IR frequency, we were not yet *"exactly"* resonant with the cooling transition. One way to ensure we are indeed frequency matched with this transition is to take advantage of the so called saturated absorption concept using a hollow cathode lamp.
The saturated absorption signal provides us with a dispersive atomic signal informing us on the detuning of the laser with respect to the cooling transition. This information we use to lock the IR laser (and therefore the blue laser) on the cooling frequency, this is done thanks to an acousto-optic modulator which specifically tunes the frequency of the IR light entering the FPC. Please see the figure 1.5 for a comprehensive locking scheme of the experiment.

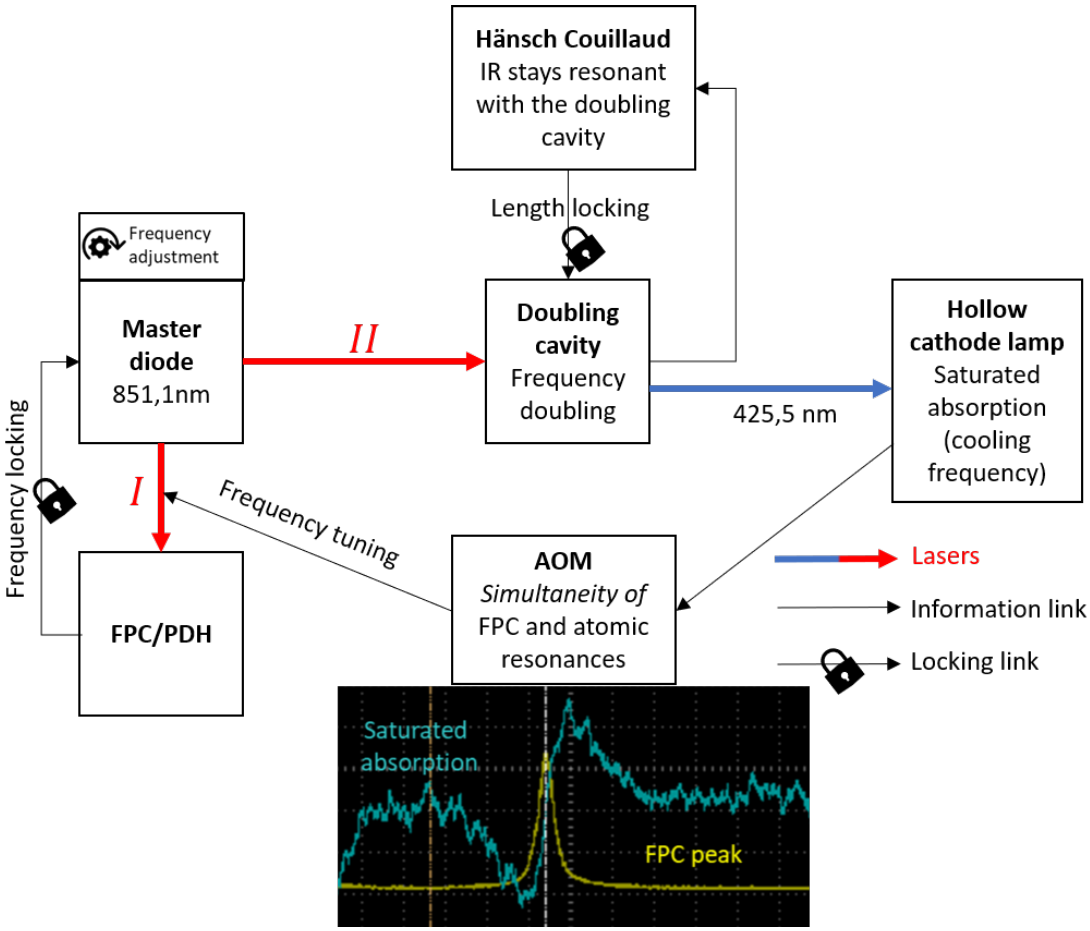

FIGURE 1.5: Locking scheme of the experiment: the IR (851.1nm) laser is divided into two parts (I and II), one of which goes through the ULE cavity and is used for frequency locking, the other goes through the doubling cavity and produces light that is frequency matched with the cooling transition. The doubling cavity's length is subjected to a servo-loop so that the incident IR light is always resonant, and thus always efficiently frequency doubled. The blue laser produced thus, goes through the hollow cathode lamp, we then finely adjust the IR frequency (Temperature, diode current, Scan control system) so that the blue laser (425.5 nm) is exactly resonant with the cooling transition. Simultaneously we use the AOM to make part I resonant with the cavity. All in all the laser is frequency locked because of part I and resonant with the cooling transition because of frequency adjustments guided by saturated absorption signal

1.6 Locking the 663nm diode

As shown in figure 1, the 663 nm diode is one of the 3 repumping lasers we use to repopulate the atomic ground state. Until recently, this diode was locked on a FPC that was itself locked using the Sa: Ti laser. This laser having become *"obsolete"*, the 663 nm diode had to be locked anew, which we did by injecting it in the same ULE cavity as the other diodes.
This locking entailed the mixing of three laser beams (the 654, 663 and 633 nm lasers). Mixing three lasers can not go without power loss, each laser relative power loss was chosen so as to optimize the final error signals. The 663 nm diode in particular was subjected to a $\simeq 70\%$ power loss.

The injection of all 3 repumping lasers into the ULE cavity brought about an unforeseen and interesting problem, that of diodes crosstalk: when all lasers are resonant, the three beams reflected off the cavity are collected by the same photodiode which generates the PDH error signals. The cross-talk happens in this photodiode.
In theory, crosstalk occurs because the discriminating electronics does not properly isolate the different modulation frequencies of each diode.
In our case the discrimination is done using a low-pass filter of the first order, and the initial modulation frequencies were 11 MHz for the 654 nm, 15 MHz for 633 nm and 10 MHz for the 663 nm diode. We thus expected that correlations would be stronger between diodes with close modulation frequencies. Surprisingly enough, perturbations did not follow this simple prediction, and did not seem in fact to depend much on the difference between modulation frequencies.

We managed to minimize the impact of these correlations on the individual error signals by regularly interspacing the modulation frequencies anyway, lowering the cutoff frequency of the low-pass filter and especially by lowering the modulation amplitude of the diodes (less RF sent to the high frequency modulation port). In particular, we checked that we could properly lock all three diodes, the concurrent functioning of all diodes being necessary to the production of chromium condensates.

Another issue related to the concurrent locking of all diodes on the same cavity was that the weak signals transmitted by the FPC from visible light diodes were drowned in the powerful one of the master diode, which made the locking all the more difficult. This issue was solved by putting up a $\lambda/4 + PBS$ system to eliminate the transmitted IR light incident on the photodiode. The IR peaks are now observed though their reflected component.

1.7 Current status of the experiment

The new MD/TA system being set, we checked that we could obtain a stable MOT with levels of fluorescence similar to those of the precedent setup (Sa: Ti).
No Bose Einstein condensate could be observed because of independents problems that occurred at the end of my training period:

- A power outage that induced a significant time delay linked to the oven temperature management and the readjustment of several experimental tools.
- Dysfunctional PDH module which was repaired.
- Failure of the 855.2 nm diode which was replaced and reinjected into a doubling cavity to produce the 427.6 nm blue depumper laser.

Chapter 2

Numerical Work

My doctoral work will focus on the study of the dynamics of entanglement growth between chromium atoms trapped in optical lattices. This growth should be characterized by the measurements of spin populations evolution. These populations are currently obtained by absorption imaging (spins are separated based on a Stern & Gerlach procedure).

Understanding the characteristics of these distributions, their first and second moments in particular, and their relationships with the experimental parameters is of utmost importance. One such parameter is the frequency of the laser used for absorption imaging.
During this internship, I investigated the impact of frequency fluctuations on the imaging of forementioned Zeeman distributions. The simulation work followed the steps below :

1. Definition of the system and Zeeman sublevels
2. Definition of the system's Hamiltonian
3. Resolution of the Bloch Optical Equations (BOE) for the 16 sublevels of the imaging transition and for arbitrary experimental parameters (Light intensity, laser frequency, magnitude of the magnetic field, light polarization)
4. Calculation of quantities relevant to the absorption imaging process, in particular the number of photons scattered during a pulse of a given duration τ
5. Evaluation of the current protocol's accuracy in determining the Zeeman populations: comparison of experimental noise due to laser frequency fluctuations to the standard quantum limit

2.1 Experimental protocol and technical noise versus standard quantum limit

In a typical experiment at t<0 the atoms of the condensate are in the $M_S = -3$ state, following the condensation, the atoms are trapped in an optical lattice, hence, they cannot move anymore, however they interact through the magnetic dipole/dipole interaction which induces spin dynamics after the spins are rotated by a radio frequency pulse. After a certain interaction time, the atoms are released and the spin populations are measured through absorption imaging. Varying the interaction time before releasing the atoms lets us retrace the interaction dynamics.

Consider then the vector state $|\psi_{\frac{\pi}{2},i}>= exp\left(-i\hat{J}_{y,i}\frac{\pi}{2}\right)|\psi_i>$, where $|\psi_i>$ is the initial vector state at t<0 of atom i, and $\hat{J}_{y,i}$ the corresponding 7×7 y-angular momentum matrix.
$|\psi_{\frac{\pi}{2},i}>$ is given by $\left\{\frac{1}{8}, \frac{\sqrt{\frac{3}{2}}}{4}, \frac{\sqrt{15}}{8}, \frac{\sqrt{5}}{4}, \frac{\sqrt{15}}{8}, \frac{\sqrt{\frac{3}{2}}}{4}, \frac{1}{8}\right\}$ in the $\hat{S}_{z,i}$ eigen-basis. If we assume the complete state describing the atoms in the condensate to be a product state (no entanglement between atoms), we can calculate the mean value of the $\hat{S}_z$ observable as such:

$$|\psi_{\frac{\pi}{2}}>= \prod_{i=1}^{N_{atom}} |\psi_{\frac{\pi}{2},i}>$$

and

$$\hat{S}_z = \sum_{i=1}^{N_{atom}} \hat{S}_{z,i}$$

So that

$$<\hat{S}_z>=<\psi_{\frac{\pi}{2}}|\hat{S}_z|\psi_{\frac{\pi}{2}}>=\sum_i <\psi_{\frac{\pi}{2},i}|\hat{S}_{z,i}|\psi_{\frac{\pi}{2},i}> = N_{atom} <\psi_{\frac{\pi}{2},1}|\hat{S}_{z,1}|\psi_{\frac{\pi}{2},1}>$$

which evaluates to zero. In the same way the variance σ^2 evaluates to $\frac{3}{2}N_{atom}$.
Considering the normalized observable $\frac{\hat{S}_z}{N_{atom}}$ (which expectation value we call magnetization in the following), we get a variance $\sigma^2 = \frac{3}{2N_{atom}}$. In other words a standard deviation for the normalized observable scaling as $\sigma = \sqrt{\frac{3}{2N_{atom}}}$. In the following this quantity will be called *Standard Quantum Noise SQN* .

In order to observe and characterize the dynamics of entanglement growth, it is necessary for the technical noise to be lower than the SQL. It is therefore desirable to lower the technical noise as much as possible.

Question:

- The current experimental noise is at least three times the SQN, can the imaging laser's frequency fluctuations explain this fact ?

This is the question I have tried to answer through the simulations which results I present below.

2.2 System, Hamiltonian and Bloch optical equations

We start by defining the system which is summarized in figure 2.1.

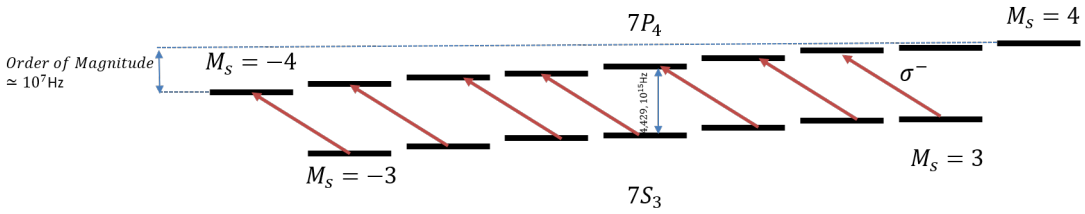

FIGURE 2.1: The system we consider in the following is the $^7S_3$ to $^7P_4$ transition of the ^{52}Cr isotope of Chromium. All relevant parameters of the atomic states are taken into account (Landé factors, energy spacing, quantum numbers, lifetimes...). The parameters of the model are the frequency detuning of the imaging laser, its intensity, its polarization, the magnetic field...

The procedure followed to define the Hamiltonian of the system is the one described in J.M Raimond's course on atoms and photons interactions ([5]). Briefly, the main idea was to adapt the known two-level system paradigm to the Chromium case by rewriting the atom-laser interaction Hamiltonian, and apply the rotating wave approximation to the Hamiltonian in the interaction picture to remove non resonant terms. From the Hamiltonian and the density matrix of the system, we generate the Bloch optical equations for ^{52}Cr. This is done by introducing terms accounting for spontaneous emission in the evolution equation of the density matrix $\left(\frac{d\rho}{dt} = -\frac{i}{\hbar}[H,\rho]\right)$. The equations are then numerically solved.
The coherence of the numerical resolution is checked in several ways, (Appendix A) amongst others, we compare the behavior of the cycling transition $M_s = -3$ to $M_s = -4$ to the behavior of a two level system. A.3

From the solution to the OBE, we calculate the number of photons scattered by a given Zeeman sublevel during an imaging pulse of duration τ: $\int_0^\tau \Gamma\rho_{excited,i}(t)$, where $\rho_{excited,i}$ is the population of the excited level as calculated by our code for the i^{th} Zeeman spot, and Γ is the lifetime of excited levels. This quantity is used afterwards to calculate the ***apparent number of atoms*** in each spot we image.

2.3 Detectivity factors and frequency drift

Consider the following picture taken in a routine measurement.

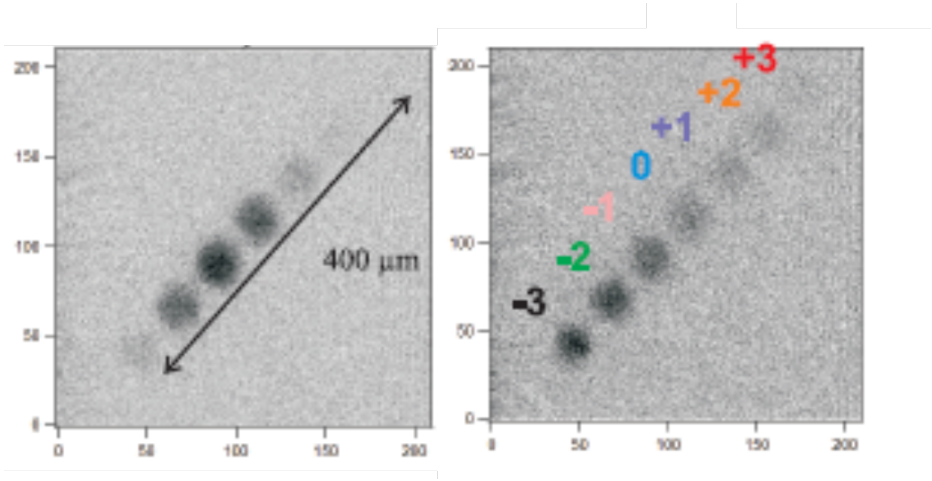

FIGURE 2.2: Left: picture of the seven Zeeman sublevels as imaged by the precedent setup, after a $\frac{\pi}{2}$ rotation and zero interaction time. Right : After a certain interaction time, evolution of the populations proves the effect of interactions.

As it turns out, despite the spin rotation operation being a well controlled technique, one does not observe the right population distribution as predicted by the $|\psi_{\frac{\pi}{2}}>$ state introduced above.
This is mainly due to the fact that not all seven states scatter light in the same way. In particular, the frequency detuning δ_0 of the laser is matched to the energy difference between magnetically shifted $^7P_3, M_s = -3$ substate and $^7P_4, M_s = -4$ substates. This means in particular that the $M_s = -3$ Zeeman sublevel/spot will scatter more light than other sublevels/spots.

In order to correct these effects, and recover the right populations, we define so-called detectivity factors, such as:

$$N_{thq,i} = N_{app,i}(\delta) * f_{M_s=i}(\delta) \;\; ; \;\; i \in [|-3;3|] \tag{2.1}$$

Where:

- $N_{thq,j}$ is the theoretical number of atoms in the j^{th} Zeeman sublevel, as such it is given by $\left|< j|\psi_{\frac{\pi}{2},i}>\right|^2 \times N_{atom}$ and **does not depend on** δ.
- $N_{app,i}(\delta)$ is the apparent number of atoms in the i^{th} Zeeman sublevel..
- δ is the frequency detuning of the laser with respect to the imaging transition

These detectivity factors are typically defined in the beginning of a series of measurements, the interaction time between atoms in the trap being null.
After calibration, the interaction time is varied and these ***initially*** defined factors are used to measure the populations dynamics.
As emphasized in the formula above, both the detectivity factors and the apparent populations are frequency dependent quantities, in actuality the detectivity factors are defined *once and for all* i.e. for an initial detuning δ_0: they are constants. The measurement of apparent populations however is sensitive to the frequency fluctuations of the laser: apparent populations are effective functions of δ.
For all intents and purposes the equation 2.1 can be rewritten :

$$N_{calculated,i}\,(\delta,\delta_0) = f_{M_s,i}(\underline{\delta_0}) * N_{app,i}(\underline{\delta}) \;\; ; \;\; i \in [|-3;3|] \tag{2.2}$$

Where now (because of frequency fluctuations) $f_{M_s,i}$ and $N_{app,i}$ are evaluated for two different detunings. Notice that N_{thq} has been replaced by $N_{calculated}$ to underline the fact that because of this δ disagreement we do not access the correct atomic populations. Hence, the bigger the frequency wander of the laser, the more severe the misevaluation of populations (the populations would be correctly evaluated for $\delta = \delta_0$), the more mistaken we are in our description of population dynamics.

In our code we use the number of photons scattered by each sublevel to access the detectivity factors $f_{M_s,i}$ and $N_{app,i}$ as functions of the detuning. The main hypothesis being that :

$$N_{app,i}(\delta) = \alpha \times N_{thq,i} \times photonscattered_i[\delta] \tag{2.3}$$

Where :

- α is a proportionality constant that does not depend on the Zeeman sublevel
- $photonscattered_i$ is the function that gives the number of scattered photons for each sublevel as explained at the end of Section 2.2

2.4 Impact of frequency drift on the evaluation of atomic populations and mean magnetization.

For more detail on the simulation scheme and results, see appendix A.
Cutting it short, we define a certain frequency fluctuation range, around the ideal detuning δ_0 , for which we calculate an initial set of detectivity factors. We then run 100 simulations each of which returns a certain detuning δ and the corresponding magnetization calculated based upon the *wrongly* corrected populations $N_{calculated}(\delta, \delta_0)$. The main results are summarized in the graph below :

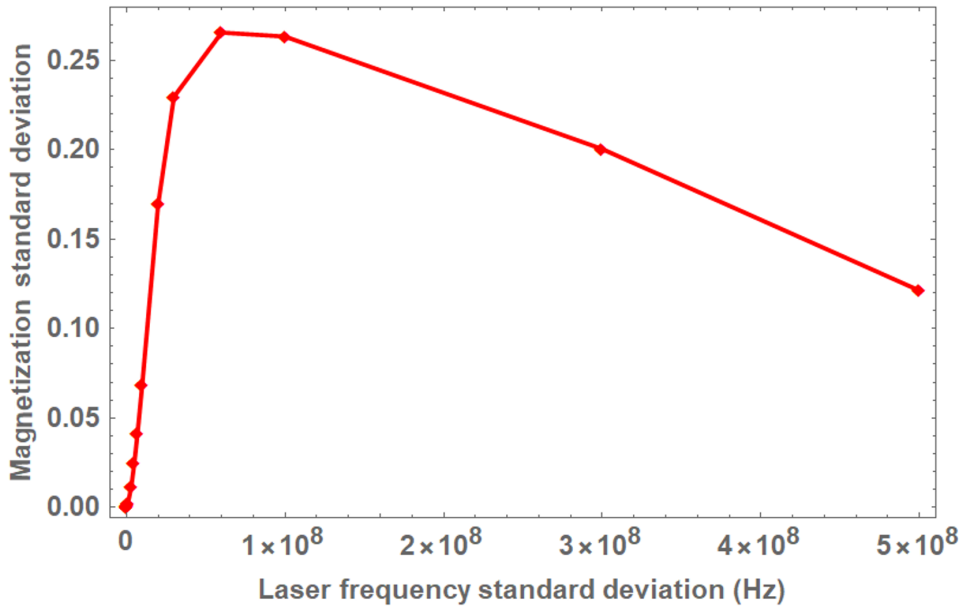

FIGURE 2.3: Final results of the simulation: the magnetization variance as a function of the laser frequency standard deviation.

In the simulation above we can see that the standard deviation of the magnetization is close to zero for small standard deviations of the laser frequency fluctuations distribution. This was to be expected as the magnetization is perfectly determined for a perfectly constant laser frequency. For large values of the laser standard deviation, the standard deviation of the magnetization decreases monotonously, this is related to the fact that the magnetization is constant for large values of the detuning (see Appendix A). In between, it reaches a maximum at 0.26, this reflects the steepness of the magnetization as a function of the laser detuning (see fig. A.4.f) .

Initial question:

- The current experimental noise is two to three times the SQN, can the imaging laser frequency fluctuations explain this fact ?

Numerical answer:

- The number of atoms trapped in a typical experiment is around 10 000, which corresponds to a SQN of 0.012, in order to obtain technical noise of three times this value through laser frequency fluctuations alone, the standard deviation of the laser should be : 6.4×10^6 Hz, which seems too be an order of magnitude bigger than the frequency fluctuations of the previous laser system (Typical laser fluctuations were estimated to $5 * 10^5$ Hz when the mechanical shutter closed).

Conclusion: It is likely that other sources of technical noise perturb the population measurements. Identifying them will be one the priorities of the beginning of my PhD.

Appendix A

Simulation supplements

A.1 supplemental verifications

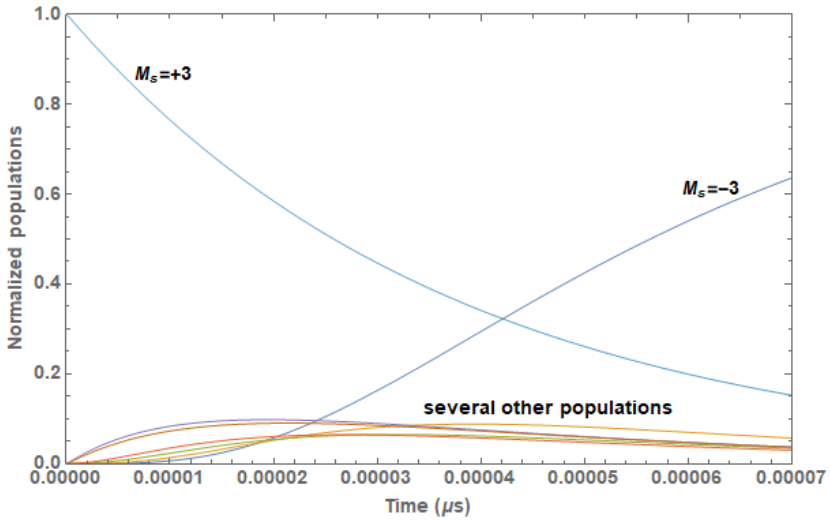

FIGURE A.1: Graph showing the optical pumping from the $M_s = +3$ state towards the M_s=-3 state for $\frac{I}{I_{sat}} = 0.05$ and a σ^- polarization, the times scales correspond with expected order of magnitudes. Several other populations are shown in the graph.

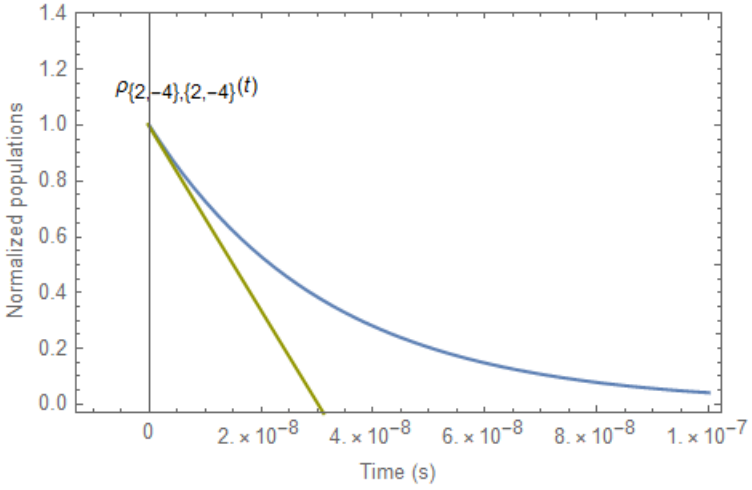

FIGURE A.2: Exponential decay of the ${}^7P_4$, $M_s = -4$ Zeeman sublevel with zero laser power. The inverse lifetime of the excited levels is $\Gamma = 2\pi * 5 * 10^6 Hz$

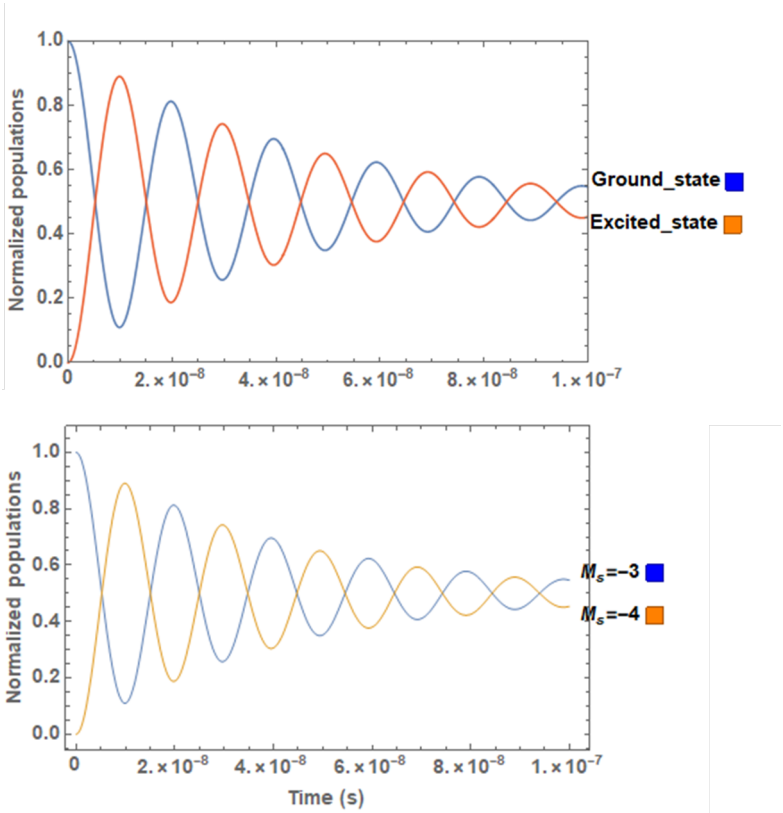

FIGURE A.3: The transition from the $^7S_3, M_s = -3$ Zeeman substate to $^7P_4, M_s = -4$ substate is closed for a incident light of left circular polarization. In other words it should behave exactly like a two level system would, which is indeed what is observed. (Up: two level system, Down: $^7S_3, M_s = -3$ to $^7P_4, M_s = -4$ transition for left circular light polarization)

A.1.1 Detectivity factors

The detectivity factors obtained through these simulations are compatible with experimental ones. For example for a pulse duration of $70\mu s$, $\alpha = 1$, B=1G, $\frac{I}{I_{sat}} = 0.05$, a detuning $\delta = -1.4 * 10^6$ Hz and a σ^- light polarization, we get the following detectivity factors.

$$f_3 = 2.24,\ f_2 = 1.26,\ f_1 = 1.05,\ f_0 = 0.97,\ f_{-1} = 0.92,\ f_{-2} = 0.89,\ f_{-3} = 0.87$$

which compare to a certain extent with typical experimental factors [4] : $f_3 = 3.73, f_2 = 3.42, f_1 = 2.81, f_0 = 2.07, f_{-1} = 1.74, f_{-2} = 1.44, f-3 = 0,98$ (Experimental parameters are not perfectly known for this precise set, in particular, it is difficult to measure experimental values of the B field's amplitude and direction during the stern & Gerlach stage). The discrepancies can be due to a number of adjustable factors, the magnetic field, the α constant, the light polarization...

A.2 Magnetization evolution with laser detuning

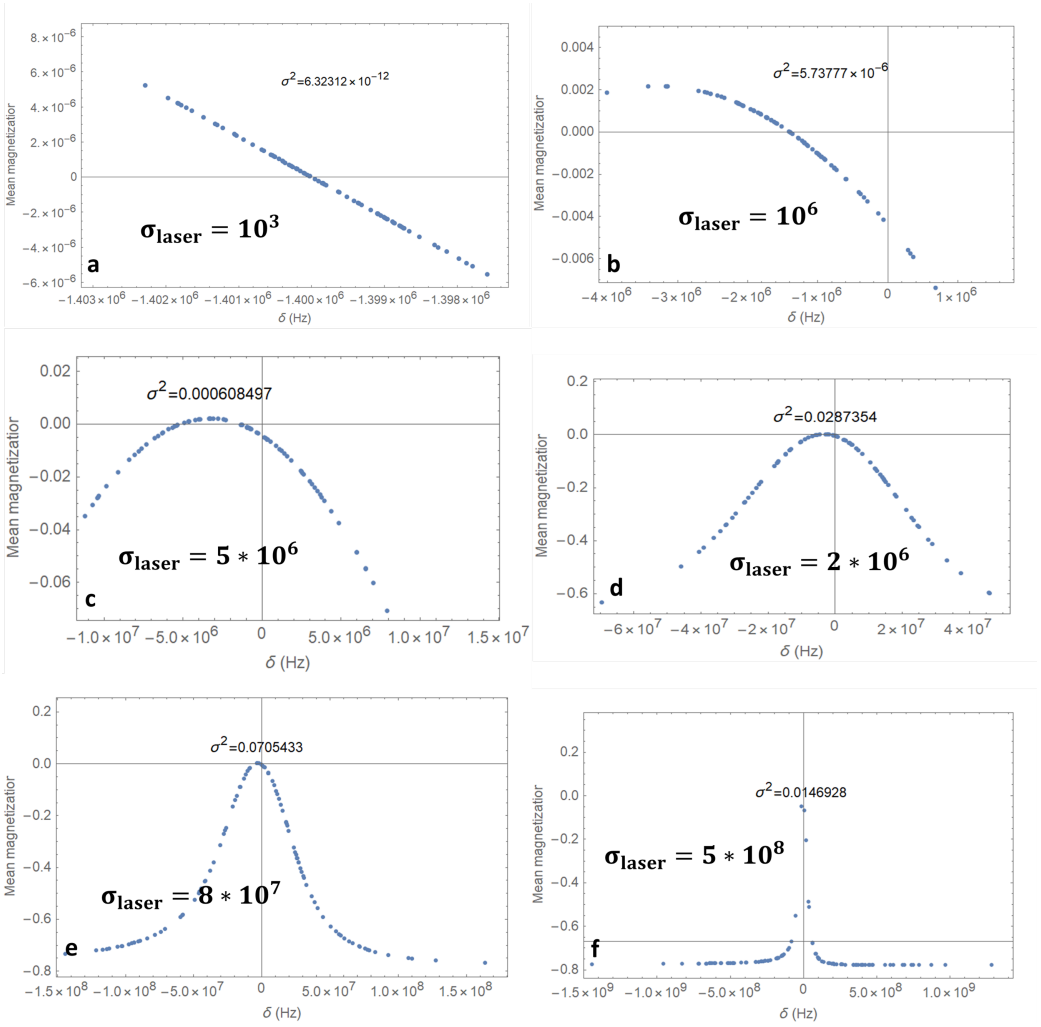

FIGURE A.4: From "a" to "f", the evolution of magnetization for an increasing range explored by the laser detuning. σ_{laser} correspond to the standard deviation of the laser, σ^2 corresponds to the variance of the magnetization distribution shown in the figure.

As the standard deviation of the laser frequency fluctuation distribution grows, the magnetization given by the sum $\sum_{i\in[-3;3]} M_{s,i} * N_{calculated,i}\,(\delta, \delta_0)$ explores a larger range of values.
In particular when the standard deviation of the laser is small (fig.a, 10^3 Hz) the magnetization shows a linear behavior around δ_0 for which it is zero as explained in sec. 2.3.
For bigger standard deviations, the magnetization is better described by a parabolic behavior (fig. b & c (MHz range)). This can be explained thus: when the detuning of the laser takes small negative values (relative to δ_0), the photon scattering rate of $M_s = -3$ decreases as the laser frequency does not match the $M_s = -3$ to $M_s = -4$ anymore. On the other hand other levels' scattering rates grow. As the detuning reaches even greater negative values, the scattering rate of $M_s = -2$ then $M_s = -1$, etc... decreases. at some point the magnetization reaches a maximum because Zeeman sublevels with positive magnetic spin moments populations are overevaluated. As the detuning reaches greater yet negative values or positive values all levels are

out of resonance with incident light, as it turns out the magnetization is negative in this case as will be explained shortly.
For even bigger standard deviations (10^7 to 10^8 Hz range), no simple fit applies to the behavior of the magnetization, but we notice that both tails of the distribution obey the same asymptotic behavior. This behavior agrees with theoretical predictions: when the laser detuning is too big, the Zeeman shift of each sublevel becomes negligible, the scattering rates ratios become proportional to the Clebsch-Gordan coefficients ratios. In the case of Chromium, the Clebsch-Gordan coefficients are as follows:

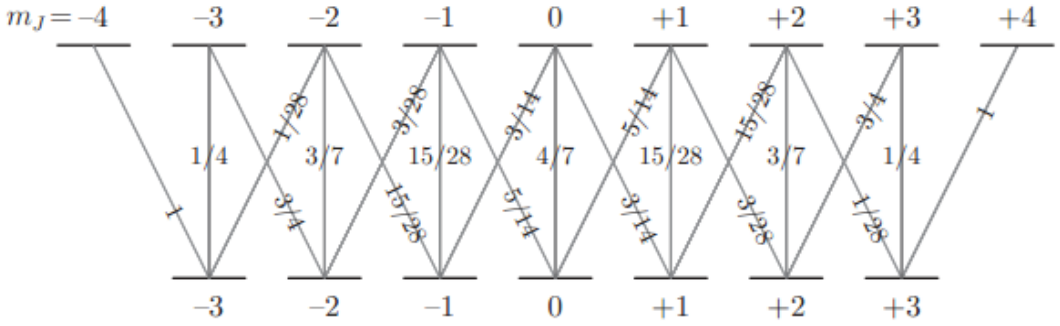

FIGURE A.5: Clebsch Gordan coefficients of ^{52}Cr. For a left circular light polarization, the *strength* of the seven transitions follow certain proportions given by: [0.035, 0.107, 0.214, 0.3571, 0.535, 0.75, 1.].
As for detectivity factors ratios, for $\delta = 10^3$ Hz we get [0.378, 0.680, 0.821, 0.896, 0.942, 0.975, 1] while for $\delta = 10^8$ we get [0.035, 0.106, 0.213, 0.356, 0.53, 0.749, 1.] which shows the announced convergence.

Therefore, when the detuning is big enough, the number of atoms in sublevels with negative magnetic spin moment is overevaluated (for a left circular light polarization), which explains the ***sign*** of the magnetization for large detunings.

Further possible developments :

- Taking into account the Doppler effect
- Investigation of the effect of light polarization on the evaluation of atom numbers
- Precise link between detectivity factors and number of scattered photons (α constant)
- Dependence of the results on the magnetic field, the light polarization, the intensity etc...

Bibliography

[1] Eric Black. *Notes on the Pound-Drever-Hall technique*. URL: https://dcc.ligo.org/public/0028/T980045/000/T980045-00.pdf.

[2] Claude Cohen-Tannoudji, Bernard Diu, and Frank Laloe. *Quantum mechanics, Volume One*. 1997.

[3] Harold J. Metcalf and Peter Vand der Straten. *Laser Cooling and Trapping*. 1999.

[4] S. Lepoutre et al. "Out-of-equilibrium quantum magnetism and thermalization in a spin-3 many-body dipolar lattice system". In: *Nature Communications* 10.1 (2019), p. 1714. ISSN: 2041-1723. DOI: 10.1038/s41467-019-09699-5. URL: https://doi.org/10.1038/s41467-019-09699-5.

[5] J.M. Raimond and H. Perrin. *Atoms and photons*. 2018.